Journal of Applied Physics

RESEARCH ARTICLE | SEPTEMBER 20 2024

Epitaxial growth of HfB_2 thin films on Si(111) by magnetron sputtering

Sathish Kumar Shanmugham; Arnaud le Febvrier ; Justinas Palisaitis ; Per O. Å. Persson ; Robert J. W. Frost ; Daniel Primetzhofer ; Ivan Petrov ; Hans Högberg ; Jens Birch; Johanna Rosen; Per Eklund ; Sanjay Nayak

J. Appl. Phys. 136, 115304 (2024)
https://doi.org/10.1063/5.0207776

AIP Publishing

Journal of Applied Physics ARTICLE pubs.aip.org/aip/jap

Epitaxial growth of HfB_2 thin films on Si(111) by magnetron sputtering

Cite as: J. Appl. Phys. **136**, 115304 (2024); doi: 10.1063/5.0207776
Submitted: 11 March 2024 · Accepted: 2 September 2024 ·
Published Online: 20 September 2024

View Online Export Citation CrossMark

Sathish Kumar Shanmugham,[1] Arnaud le Febvrier,[1,a)] Justinas Palisaitis,[1] Per O. Å. Persson,[1] Robert J. W. Frost,[2] Daniel Primetzhofer,[2,3] Ivan Petrov,[1,4] Hans Högberg,[1] Jens Birch,[1] Johanna Rosen,[5] Per Eklund,[1] and Sanjay Nayak[1,a)]

AFFILIATIONS

[1]Thin Film Physics Division, Department of Physics, Chemistry, and Biology (IFM), Linköping University, SE-581 83, Linköping, Sweden
[2]Tandem Laboratory, Uppsala University, Uppsala, SE 75120, Sweden
[3]Division of Applied Nuclear Physics, Department of Physics and Astronomy, Uppsala University, Uppsala, SE 75120, Sweden
[4]Frederick Seitz Materials Research Laboratory and Department of Materials Science, University of Illinois, Urbana, Illinois, 61801, USA
[5]Materials Design Division, Department of Physics, Chemistry, and Biology (IFM), Linköping University, SE-581 83, Linköping, Sweden

[a)]**Authors to whom correspondence should be addressed:** arnaud.lefebvrier@liu.se, sanjay.nayak@liu.se, and sanjaynayak.physu@gmail.com

ABSTRACT

Hafnium diboride (HfB_2) is a promising candidate as a seed layer for GaN growth on Si substrates due to its excellent lattice and thermal coefficients matching with both materials. This work investigates the epitaxial growth of AlB_2-type non-stoichiometric HfB_2 ($HfB_{2+\delta}$ with $-0.1 < \delta < 0.6$) thin films on Si(111) using magnetron co-sputtering. We demonstrated that the process temperature significantly affected the surface roughness ($R_{RMS} \sim 0.5$–4 nm), film composition, and the nucleation of secondary impurity phases. Films deposited between 700 and 900 °C exhibit epitaxial growth on the Si substrate with a well-defined relationship of $(0001)_{HfB2}\|(111)_{Si}$ and $[11\bar{2}0]_{HfB2}\|[1\bar{1}0]_{Si}$. Detailed x-ray diffraction and scanning transmission electron microscopy analyses reveal that impurity phases detected at high temperatures are primarily carbon-rich phases, identified as HfC_x or HfC_xB_y. Interestingly, this secondary phase's crystal orientation follows the orientation of its surroundings. The different findings in terms of contamination (C and O) and deposition temperature offer valuable insights for further growth optimizing of high-quality epitaxial HfB_2 thin films on Si(111) for future GaN-on-Si integration.

INTRODUCTION

Transition metal diborides (TMB_2) are of interest due to their combination of mechanical, chemical, thermal, and electrical properties.[1–3] TMB_2 are, in many cases, also ultrahigh-temperature ceramics with high melting points and chemical and oxidation resistance, which make them of interest for applications such as cutting and drilling tools, wear-resistant coatings, hypersonic vehicles, and diffusion barriers in integrated circuits.[4–7] The synthesis and materials' properties binary of TMB_2 compounds, such as titanium diborides (TiB_2), zirconium diboride (ZrB_2), and chromium diboride (CrB_2), in thin film form have been studied,[8–16] while hafnium diboride (HfB_2) has received less attention despite it being considered to exhibit high oxidation resistance and superior hardness (47.7 ± 2.7 GPa) among binary metal diborides.[17–20] The bulk material lattice parameters of AlB_2-type HfB_2 are similar to those of GaN ($a_{HfB2} = 3.15$ Å, $a_{GaN} = 3.19$ Å), suggesting that HfB_2 could also serve as a buffer layer on Si(111) for the epitaxial growth of GaN and AlGaN films.[21,22] Epitaxial films of materials are also desirable for exploring their anisotropic nature of physical and

chemical properties.[23,24] However, the growth of epitaxial HfB_2 thin films using chemical vapor deposition and/or physical vapor deposition techniques has been a challenging task.[25–29]

Roucka *et al.*[30] demonstrated epitaxial growth of $Hf_xZr_{1-x}B_2$ on the on-axis and vicinal miscut of Si(111) surfaces using bimolecular reactions of $Hf(BH_4)_4$ and $Zr(BH_4)_4$ in an ultrahigh vacuum system. The depositions were carried out at 900 °C with a low growth rate of 0.5 nm/min. Furthermore, the epitaxial HfB_2 films on a bare Si(111) substrate developed by Roucka *et al.*[31] showed very high surface roughness (>15 nm), which is reduced upon growing on a ZrB_2 buffer layer, but the substrate temperature remains still high to achieve epitaxy with a very low growth rate. This gas phase epitaxy growth technique is expensive and challenging to achieve high-throughput industrial production. On the other hand, thin film growth by magnetron sputtering, used here, is known to be scalable with high-throughput production capabilities. Additionally, epitaxy can be achieved by sputter deposition at a lower substrate temperature compared to MOCVD or gas phase epitaxy techniques. Low-temperature growth processes are preferred over high temperature, as the latter promotes impurity incorporation,[32] film–substrate interdiffusion,[33] and higher thermal stress.[34]

Many failed attempts were made in the past for the growth of epitaxial thin films of HfB_2 using magnetron sputtering.[18,35,36] Recently, we have demonstrated the epitaxial growth of ZrB_2 using co-sputtering, achieving epitaxy at 200 °C lower than what could be achieved with sputtering from a compound target[12] and by chemical vapor epitaxy techniques. Thus, we envisage that the co-sputtering of hafnium and boron can be a path for the growth of epitaxial HfB_2 thin films.

Herein, we report on the successful growth of epitaxial AlB_2-type $HfB_{2\pm\delta}$ thin films on Si(111) substrates as obtained by magnetron sputtering using hafnium and boron elemental targets in a temperature regime between 700 and 900 °C. The influences of the substrate temperature on crystallographic texture, surface morphology, crystallinity, and composition are characterized.

EXPERIMENTAL DETAILS

$HfB_{2\pm\delta}$ thin films were deposited by magnetron co-sputtering using elemental targets of hafnium [Plasmaterials Inc., 99.9% purity (excluding Zr), 50. 8 mm in diameter] and boron (Testbourne Ltd., 99.99% purity, 50. 8 mm in diameter) in an ultrahigh vacuum deposition system with a base pressure of 2×10^{-9} mbar. The Zr impurity concentration in the Hf metal target is expected to be within 3 at. %. The targets were situated at 140 mm and an angle of 30° from the substrate. The system is described in detail elsewhere.[37] All films were deposited onto 10×10 mm^2 Si(111) substrates, which were ultrasonically cleaned with acetone and isopropanol for 10 mins and blown dry with pure nitrogen before insertion in the chamber. The substrates were annealed at the respective deposition temperature for 60 mins before deposition for temperature stabilization. During the deposition process, the argon flow rate was kept constant at 45 SCCM, which corresponded to a pressure of 3.3×10^{-3} mbar. RF magnetron sputtering was used for the two boron targets with the DC equivalent RF power set to 64 W, while DC magnetron sputtering was used to power the hafnium target at a power of 5 W. Prior to film deposition, the targets were pre-sputtered for 20 mins under the same conditions as for the deposition. The substrate stage was kept under a constant rotation of 45 rpm without any external electrical substrate bias (i.e., at floating potential). The thin films were grown at four different substrate temperatures (T_s) of 500, 700, 800, and 900 °C.

The crystal structure was characterized by Bragg–Brentano x-ray diffraction (XRD) θ–2θ scans using a Philips PW 1820 system with a Cu-Kα source operated at 45 kV and 40 mA. XRD pole figure measurements were performed in a Philips X'Pert MRD system operated at 45 kV and 40 mA with a Cu-Kα source with angular step sizes of 2° and 5° at tilt angle Ψ and azimuth angle φ, respectively. The thickness of the films was determined from x-ray reflectivity (XRR) measurements and analyzed using the X'pert Reflectivity program. The chemical compositions of the films were determined using the combined techniques of Rutherford backscattering spectrometry (RBS) and time-of-flight Elastic Recoil Detection Analysis (ToF-ERDA). The RBS measurements were performed with a 2 MeV helium beam with an incident angle of 5° to the surface normal, while the detector is at a scattering angle of 170°. The SIMNRA software package[38] was used for the simulation and analysis of the RBS spectrum. ToF-ERDA measurements were carried out in a tandem accelerator[39,40] with a 36 MeV $^{127}I^{8+}$ primary-ion beam at an incidence angle of 67.5° to the sample normal and recoils detected at an angle of 45° to the primary beam. The measured ToF-ERDA spectra were converted into depth-dependent relative atomic concentration profiles using the Potku software,[41] and a more in-depth analysis was then performed using the MCERD simulation[42] package that comes with Potku.

Cross-sectional scanning transmission electron microscopy (STEM) analyses were carried out in a Linköping monochromated and double-corrected FEI Titan^3 60–300 electron microscope operated at 300 kV. TEM specimens were prepared by mechanical polishing, followed by Ar^+ ion milling at 5 keV, with a 5° incidence angle, on both sides of each sample during rotation, in a Gatan precision ion polishing system (PIPS). The specimens were finally sputter-cleaned using an ion energy of 0.5 keV without changing the angle of incident of Ar^+ ions.

A Bruker Dimension 3100 atomic force microscope (AFM), operated in the tapping mode, was used to characterize the surface morphology and roughness of each sample. The data were processed with the WSXM analysis software.[43]

RESULTS

X-ray θ–2θ diffraction patterns of the Hf-B films deposited at different temperatures are shown in Fig. 1. For all the samples, two sharp peaks at $2\theta \approx 28.4°$ and 58.9° corresponded to the substrate peaks of Si 111 and Si 222, respectively.[44] For the sample grown at $T_s = 500$ °C, no other peaks than the substrates peaks were visible, indicating that the film is x-ray amorphous. For a growth temperature of 700 °C, two additional intense Bragg peaks are observed at $2\theta = 25.8°$ and 52.7°. These peaks are identified as the diffraction peaks of 0001 and 0002 of the AlB_2-type HfB_2.[45] The diffractogram also shows a broad peak at $2\theta = 58.7°$, which matches $(11\bar{2}0)$ HfB_2 and overlaps with the Si 222 peak at $2\theta = 58.9°$. In addition, a monoclinic HfO_2 phase was detected with a peak at a 2θ angle of 49.6° corresponding to its (220) plane.[46] The formation of the

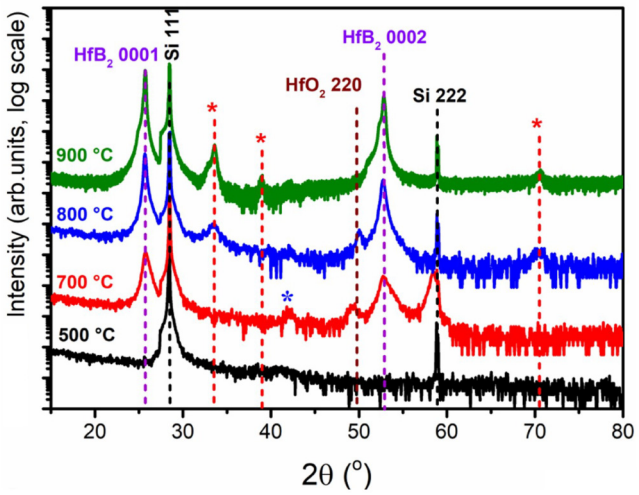

FIG. 1. X-ray diffractograms of $HfB_{2\pm\delta}$ thin films deposited at various substrate temperatures. The peaks are labeled with the corresponding compounds and hkl values, while the unidentified peaks are marked with "*".

monoclinic phase HfO_2 within the HfB_2 matrix is consistent with the observation made by Glechner *et al.*[20] during an oxidation kinetics study. The film deposited at 800 °C had similar features, with the 000l preferential orientation along the growth direction and the presence of HfO_2. The crystal quality of the HfB_2 phase is enhanced at 800 °C compared to the one deposited at 700 °C, as shown by the increased intensity and reduced peak width of the 0001 and 0002 peaks. At 900 °C, prominent peaks from HfB_2 exhibit a similar intensity compared with the (111) and (222) peaks from the Si substrate, indicating an improved crystal quality of the HfB_2 phase. No peaks from oxides can be observed, contrary to the films deposited at lower temperatures. The formation of HfO_2 at 700 and 800 °C could be the result of the reaction of incoming hafnium atoms, with the native oxide layer left on the silicon substrate. This native oxide layer on Si seems to be removed by the initial annealing at 900 °C for 60 min as no oxide phases were detected for that deposition of temperature. The diffractograms of the films deposited at the 800 and 900 °C samples reveal the presence of a secondary phase with peaks at $2\theta = 33.6°$, 38.9°, and 70.6° that closely match with 111, 200, 220, and 222 reflections of both rock salt (space group: $Fm\bar{3}m$) HfB as well as HfC.[47,48] From XRR, the deposition rates for all four films were determined to be 0.75 nm/min, i.e., the overall thickness of all the films is approximately 50 ± 5 nm.

Figure 2 shows the compositions of the films as evaluated by a combination of ToF-ERDA [Fig. 2(a)] and RBS measurements [Fig. 2(b)]. The contents of low-mass impurity elements such as carbon, nitrogen, and oxygen were determined from ToF-ERDA measurements and were used in the fitting of RBS spectra in determining the overall compositions of the films. The RBS spectrum shows that the only detectable metal contaminant is zirconium at a level below 1 at. %, which is the usual metallurgical impurity in Hf. While oxygen is detected by the ToF-ERDA [Fig. 2(a)], a more detailed analysis of the data using MCERD (example in Fig. 3)

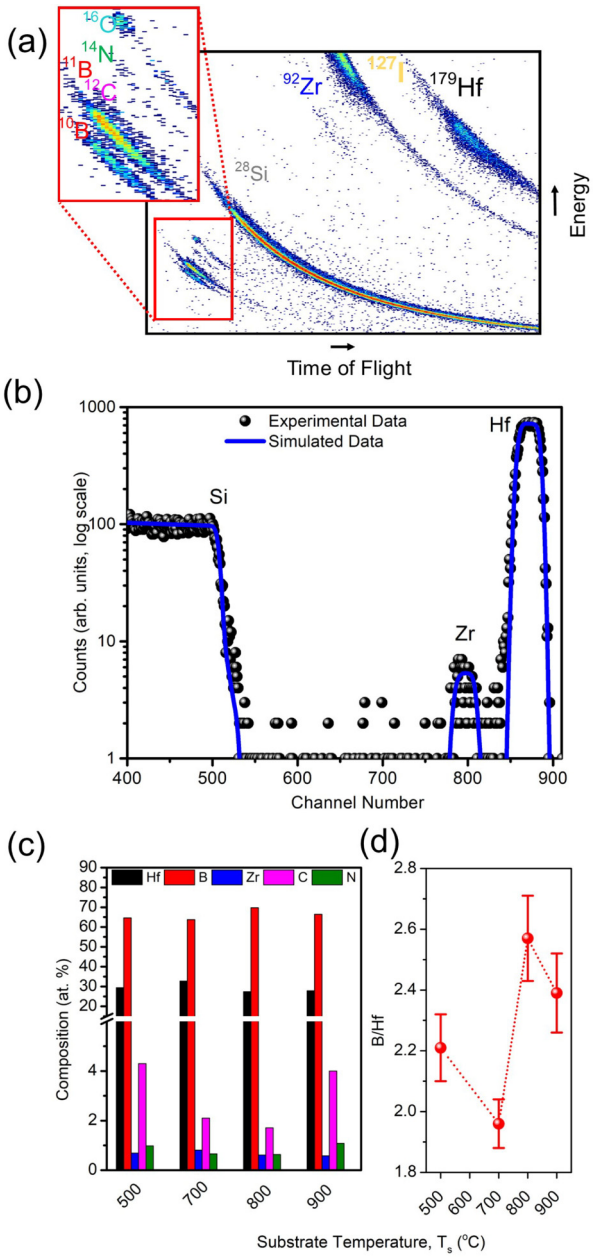

FIG. 2. (a) Time-of-flight (ToF) energy coincidence plot recorded in elastic recoil detector analysis (ERDA) for the film deposited at a substrate temperature of 800 °C. (b) Rutherford backscattering (RBS) data for the same film. (c) Composition of the films as obtained by combining ERDA and RBS analysis and (d) B/Hf ratio.

shows that this is localized at the surface and at the film–substrate interface. The localization of oxygen at the surface and interface likely results from postdeposition surface oxidation and from the Si native oxide prior to deposition not entirely removed at a

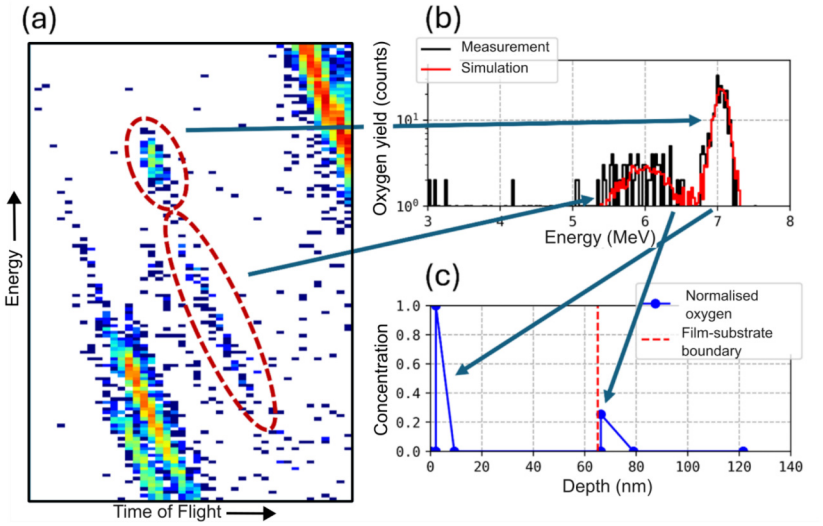

FIG. 3. Illustration of the MCERD analysis of oxygen localization for the film deposited at a substrate temperature of 800 °C. (a) The ToF-ERDA spectra [also in Fig. 2(a)] with the data points for oxygen highlighted. (b) The projected energy spectrum from a cut made to the oxygen data points in (a), alongside the simulated energy spectrum obtained by assuming the distribution of oxygen shown in (c). The accuracy of the depth scale in (c) is limited by uncertainties in the surface edge calibration, the density of the film, and the stopping-power tables used by the analysis algorithm.

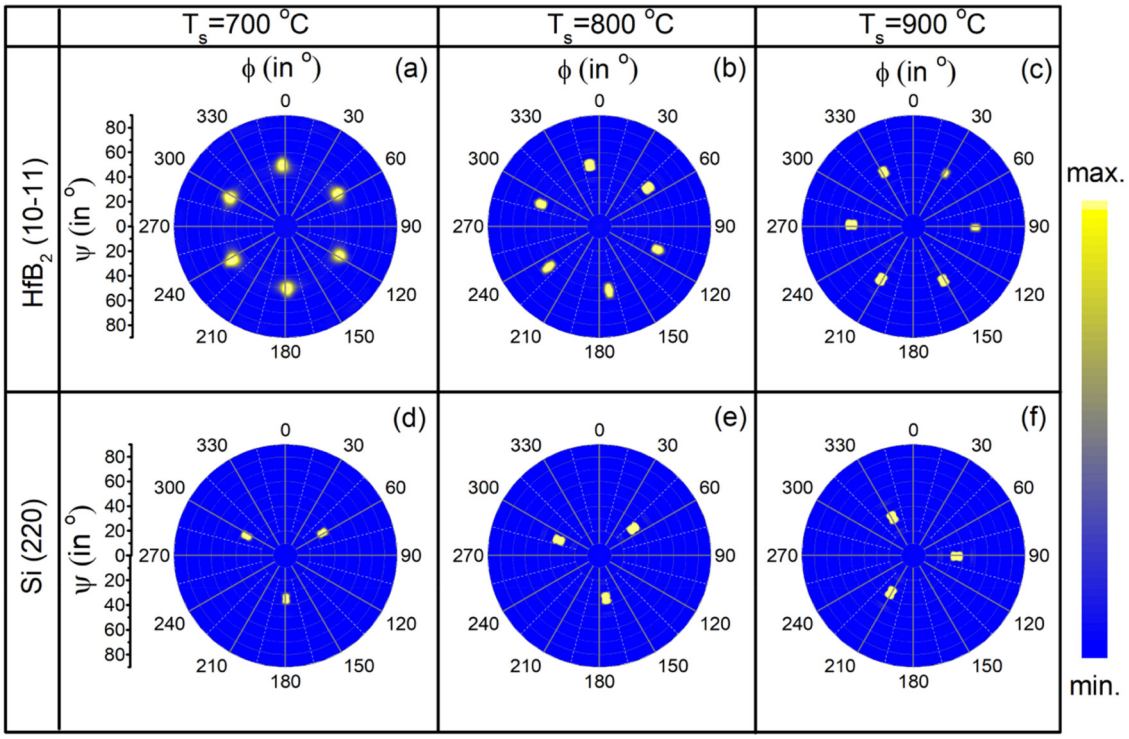

FIG. 4. Pole figures of $HfB_{2\pm\delta}$ films grown on Si(111) at substrate temperatures of 700, 800, and 900 °C. (a)–(c) The pole figure of the $HfB_{2\pm\delta}$ $10\bar{1}1$ reflection at $2\theta = 42.2°$, and (d)–(f) the pole figure of Si 220 reflection at $2\theta = 47.3°$.

deposition temperature of 800 °C. The decrease in XRD peak intensity when the substrate temperature increases is explained by the removal of the native oxide during the annealing of the substrate prior to deposition. Any oxygen concentration in the bulk of the films is below the limits of detection <0.1 at. %. The contents of boron/hafnium (B/Hf) in samples grown at 500, 700, 800, and 900 °C were 2.21 ± 0.11, 1.96 ± 0.08, 2.57 ± 0.14, and 2.39 ± 0.13, respectively (Fig. 2). Therefore, close to stoichiometry, borides were grown at 700, while boron-rich films were grown at 500, 800, and 900 °C.

To examine the texture and epitaxy of the films, XRD pole figure measurements were carried out at $2\theta = 47.30°$ and 42.2°, i.e., the angular positions corresponding to diffraction from lattice planes of Si(220) and $HfB_2(10\bar{1}1)$, respectively. The pole figures of the $(10\bar{1}1)$ pole of HfB_2 measured for the films grown at $T_s = 700$, 800, and 900 °C, HfB_2 $(10\bar{1}1)$ are shown in Figs. 4(a)–4(c), respectively, and the corresponding pole figures for Si (220) poles are shown in Figs. 4(d)–4(f). The $(10\bar{1}1)$ pole figure of HfB_2 [Figs. 4(a)–4(c)] shows six equidistant poles at $\Psi \sim 50°$ separated by 60° φ, a consequence of an epitaxial growth with a sixfold symmetry of the families of planes from AlB_2-type HfB_2. The pole figure of the substrates [Figs. 4(d)–4(f)] shows three distinct poles separated by 120° in φ and at a Ψ angle of ~35°originating from Si (220) planes yielding the following epitaxial relationship with the film: $(0001)_{HfB2} \| (111)_{Si}$ and $[11\bar{2}0]_{HfB2} \| [1\bar{1}0]_{Si}$.

Figure 5 shows the STEM micrographs from the film grown at 900 °C and reveals the presence of angular grains. These crystalline grains or domains appear with different contrasts and seem to be specifically oriented. An extended investigation revealed that the inclusions appearing/nucleating in the midst of the film have a specific orientation compared to the growth direction [Fig. 5(c)]. In contrast, inclusions appearing at the substrate/film interface show no specific orientation [Fig. 5(b)]. All other crystalline domains (not inclusions) were identified as the AlB_2-type HfB_2 phase consistent with the XRD results.

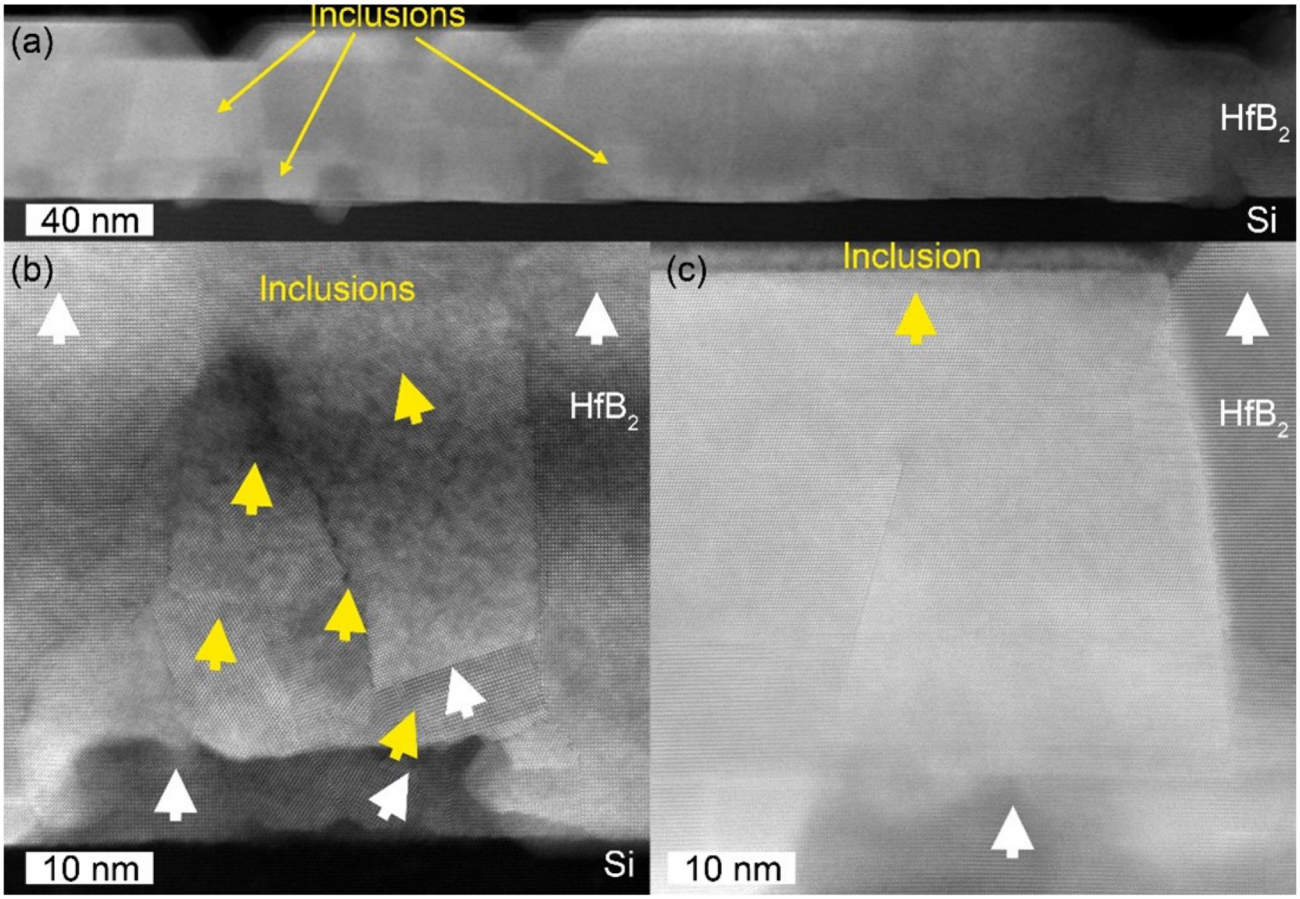

FIG. 5. Cross-sectional STEM micrographs of a $HfB_{2\pm\delta}$ film deposited on Si(111) at 900 °C. (a) An overview image from the $HfB_{2\pm\delta}$ film. HRTEM image showing the orientation of inclusions starting close to the substrate/film interface (b) and embedded into the grown film (c). Arrows (yellow) marked the regions of inclusions and their corresponding orientation with respect to the surrounding film.

Figure 6 shows the Hf-L_α energy-dispersive x-ray spectroscopy (EDX), and C-K, and B-K electron energy loss spectroscopy (EELS) elemental maps acquired from a zone containing one of the inclusions. The local analysis reveals that carbon was detected within the inclusion [Fig. 6(c)], while boron [Fig. 6(d)] appears in the ambient film and is absent within the inclusion.

Figure 7(a) represents the cross-sectional STEM images showing the atomic structure of the interface between the HfB_2 thin film and Si substrate (along the [1$\bar{1}$0] Si zone axis). Figure 7(a) shows a homogeneous and dense HfB_2 film directly and epitaxially grown on a Si substrate without the presence of a native silicon oxide layer. Note here that the zone axis for the HfB_2 layer is along its [11$\bar{2}$0] direction. Closer observations reveal the presence of a surface step on the Si substrate. These results confirm the observation done by Pole figure XRD analysis where the following epitaxial relationship was established: $(0001)_{HfB2}\|(111)_{Si}$ and $[11\bar{2}0]_{HfB2}\|[1\bar{1}0]_{Si}$. Figure 7(b) shows the atomically resolved STEM images from both inclusion and the surrounding film recorded from a region where both were present. The local fast Fourier transformation (FFT) of the respective domains revealed that the inclusions are the rock salt phase along its [1$\bar{1}$0] zone axis, while the HfB_2 was AlB_2-type along its [11$\bar{2}$0] zone axis (Fig. 7). The interplanar spacing, as measured from the FFT of the images, of the rock salt phased domain parallel to the film/substrate interface is 2.5 Å. This interplanar spacing matches the *d*-spacing for 111 crystal planes of rock salt HfC.[48] Thus, the spatially resolved elemental maps (Fig. 6) and STEM images (Fig. 7) confirmed that the inclusions were HfC or carbon-rich $HfB_{1-x}C_x$. The HRTEM data show that for many rock salt HfC domains, (111) planes are perfectly aligned along the growth direction. This establishes an epitaxial relationship of $(111)_{HfC}\|(0001)_{HfB2}$ and $[1\bar{1}0]_{HfC}\|[11\bar{2}0]_{HfB2}$. Thus, the observed XRD peaks at $2\theta = 33.6°$, 38.9°, 56.2°, and 70.6° were confirmed to be the 111, 200, 220, and 222, respectively, reflections from rock salt HfC/carbon-rich $HfB_{1-x}C_x$. The growth of epitaxial or highly oriented rock salt HfC domains explains the high-intensity XRD peak obtained (Fig. 1) despite the very low carbon content (and, hence, low fraction of rock salt HfC domain) in the film.

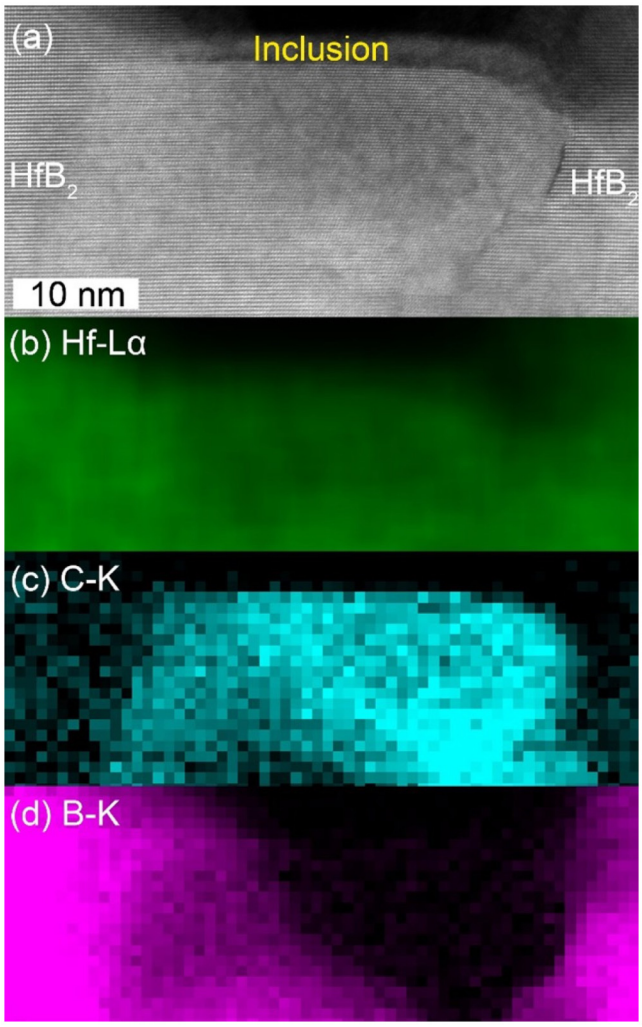

FIG. 6. (a) STEM image of an isolated inclusion close to the film surface. (b) The EDX elemental distribution map of hafnium (Hf-L_α). (c) C-K and (d) B-K EELS elemental maps for carbon and boron, respectively.

The incorporation of carbon impurities in HfB_2 is not well understood yet. The phase-diagram of Hf-B-C up to ~900 °C was not thoroughly investigated in the literature. Based on thermodynamic calculations, Rogl and Bittermann[49] suggested that the segregated HfB_2 and C phases as well as segregated HfB_2 and B_4C phases would remain thermodynamically stable, and no reaction would be expected at temperatures below 2600–2800 K. However, *ab initio* methods showed that a high carbon content ($x = 0.5$) in $HfB_{1-x}C_x$ would decompose into AlB_2-type HfB_2, rock salt HfC, and monoclinic B_4C (space group: C1m1).[50,51] Our recent work also showed that carbon incorporation by insertion/dilution into an AlB_2-type ZrB_2 was a thermodynamically unfavored process.[12] Since the growth temperatures here (800–900 °C) were high enough for carbon atoms to achieve a higher diffusion length, there is a strong possibility of their reaction with hafnium adatoms, followed by nucleation in the rock salt HfC domain.[52] The residual carbons from the magnetron target materials were the likely sources of carbon in these samples.

To examine the effect of the substrate temperature on the surface morphology of the films, atomic force micrographs were obtained (Fig. 8). The root-mean-square (RMS) surface roughness (R_{RMS}) obtained from scanned AFM topography over the $3 \times 3\ \mu m$ was 0.52, 1.38, 2.63, and 3.97 nm for films deposited at 500, 700, 800, and 900 °C, respectively. The increase in surface roughness with a higher substrate temperature was mainly attributed to an increase in the adatom energy at a higher temperature yielding larger domains in the oriented films and faceted surfaces as well as the formation of phase segregated induced roughness.[53,54]

The present study shows that by co-sputtering, the epitaxial growth of $HfB_{2+\delta}$, with $-0.1 < \delta < 0.6$, on Si(111) substrates can be achieved at 700 °C, which is almost 200 °C lower than the typical

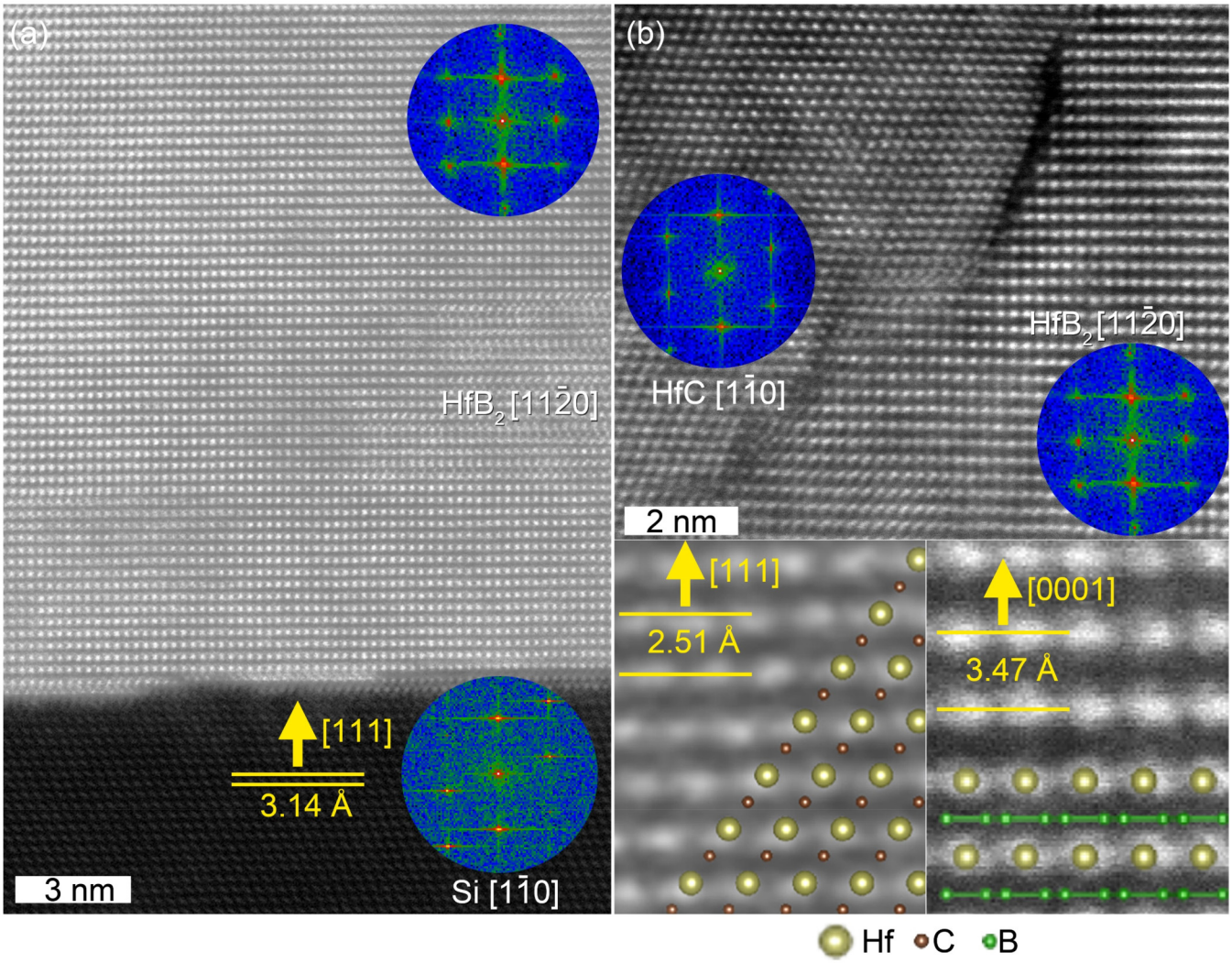

FIG. 7. Atomically resolved STEM image showing (a) the interface between HfB_2 and the Si substrate along the [1$\bar{1}$0] Si zone axis. (b) Rock salt HfC inclusion embedded into the AlB_2-type HfB_2 surrounding film. Corresponding FFT patterns and interplanar spacings of HfC and HfB_2 atomic models overlayed along [1$\bar{1}$0] and [11$\bar{2}$0] zone axes, respectively. The yellow lines serve as a guide.

temperature required using CVD.[25] Our work also shows the effect of substrate temperature on the stoichiometry and impurity incorporation in HfB_2 in a sputtering process. The oxygen contamination leading to local oxide formation at the interface was attributed to the diffusion from the presence of the native oxide on the Si substrate prior to deposition. Nevertheless, no oxide or oxygen contamination was detected after the removal of silicon native oxide by annealing in vacuum. The residual carbon contamination at a level of 2–4 at. % in HfB_2 was most likely incorporated during growth originating from the target. At high substrate temperatures, the residual carbon forms highly oriented HfC or carbon-rich $HfB_{1-x}C_x$ and results in secondary phase formation.

Growth of epitaxial HfB_2 is challenging and has been reported to be achievable by CVD at high temperatures[17,30,31,55–57] while we have demonstrated the capability of using magnetron sputtering for it at lower temperatures and using the elemental target. These results underline the high prospects on the growth of HfB_2 using magnetron sputtering, which is a process scalable and with a high-throughput production. We also highlighted the main concerns for the growth of HfB_2 by magnetron sputtering, specifically addressing carbon and oxygen contamination to prevent the formation of secondary phases such as HfO_x and HfC_x. In order to reduce such contamination for a HfB_2 sputtered film, the use of a UHV chamber is necessary along with the reduction of any source of contaminants such as oxygen and carbon impurities.

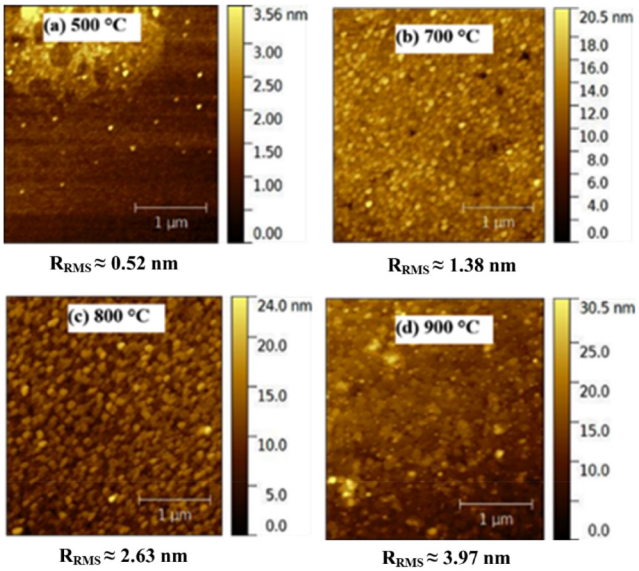

FIG. 8. Atomic force microscopy (AFM) images of $HfB_{2\pm\delta}$ thin films at 500 (a), 700 (b), 800 (c), and 900 °C (d) growth temperatures. The RMS roughness (R_{RMS}) values of the films are also indicated below the respective figures.

CONCLUSIONS

In summary, we show that epitaxial $HfB_{2+\delta}$, with $-0.1 < \delta < 0.6$, thin films on Si(111) substrates can be achieved by magnetron co-sputtering from elemental targets of hafnium and boron. The epitaxial relationship is $(0001)_{HfB2}\|(111)_{Si}$ and $[11\bar{2}0]_{HfB2}\|[1\bar{1}0]_{Si}$. Our results show a strong influence of the substrate temperature on crystalline quality and surface morphology, as well as the composition of the films and incorporation of impurities. The films grown at a substrate temperature of 700 °C and above are composed of AlB_2-type HfB_2 and remained epitaxial despite the compositional fluctuations in boron around the stoichiometry. Composition depth profiling using ERDA and RBS revealed the presence of 3–5 at. % of carbon contaminant in all films, which played a critical role in the phase composition in the film. At high temperatures and with the presence of C contamination (<4–5 at. %), a secondary rock salt $HfC/HfB_{1-x}C_x$ formed as inclusions. The results suggest that the growth temperature and the carbon contaminants are critical factors for controlling the phase purity and microstructure of HfB_2 thin films. From the AFM studies, it was found that the RMS roughness and grain size of the thin films increase with the increase in the substrate temperature. This work highlighted the high prospect for using magnetron sputtering to deposit diboride epitaxial films, which can be used as a template for GaN growth on Silicon. Nevertheless, careful control of contaminants is needed to achieve the phase pure epitaxial growth of HfB_2 on silicon substrates using magnetron sputtering.

ACKNOWLEDGMENTS

We acknowledge the support from the Knut and Alice Wallenberg (KAW) Foundation for project funding through The Boride Frontier (No. KAW 2015.0043), Academy Fellow (No. P.E. 2020.0196), and Scholar (No. J.R. 2019.0433). Accelerator operation was supported by the Swedish Research Council VR-RFI (Contract No. 2019-00191). Swedish Research Council (VR) and Swedish Foundation for Strategic Research (SSF) are acknowledged for access to ARTEMI and the Swedish National Infrastructure in Advanced Electron Microscopy (Nos. 2021-00171 and RIF21-0026).

AUTHOR DECLARATIONS

Conflict of Interest

The authors have no conflicts to disclose.

Author Contributions

Sathish Kumar Shanmugham: Conceptualization (lead); Data curation (lead); Formal analysis (lead); Investigation (supporting); Methodology (lead); Supervision (supporting); Validation (equal); Writing – original draft (lead); Writing – review & editing (equal). **Arnaud le Febvrier:** Conceptualization (equal); Data curation (lead); Formal analysis (lead); Investigation (supporting); Methodology (supporting); Supervision (supporting); Validation (equal); Writing – original draft (equal); Writing – review & editing (equal). **Justinas Palisaitis:** Data curation (lead); Formal analysis (lead); Investigation (supporting); Methodology (supporting); Writing – review & editing (equal). **Per O. Å. Persson:** Conceptualization (supporting); Funding acquisition (equal); Investigation (supporting); Validation (supporting); Writing – review & editing (equal). **Robert J. W. Frost:** Data curation (lead); Formal analysis (lead); Investigation (equal); Writing – review & editing (equal). **Daniel Primetzhofer:** Data curation (supporting); Funding acquisition (supporting); Investigation (supporting); Validation (supporting); Writing – review & editing (supporting). **Ivan Petrov:** Conceptualization (equal); Investigation (equal); Methodology (supporting); Validation (supporting); Writing – review & editing (equal). **Hans Högberg:** Conceptualization (supporting); Funding acquisition (supporting); Investigation (supporting); Writing – review & editing (supporting). **Jens Birch:** Conceptualization (equal); Investigation (supporting); Methodology (supporting); Writing – review & editing (supporting). **Johanna Rosen:** Conceptualization (equal); Funding acquisition (lead); Investigation (equal); Methodology (supporting); Supervision (lead); Writing – review & editing (equal). **Per Eklund:** Conceptualization (equal); Funding acquisition (lead); Investigation (equal); Supervision (lead); Writing – review & editing (equal). **Sanjay Nayak:** Conceptualization (lead); Data curation (lead); Formal analysis (lead); Investigation (lead); Methodology (lead); Validation (equal); Writing – original draft (equal).

DATA AVAILABILITY

The data that support the findings of this study are available from the corresponding authors upon reasonable request.

REFERENCES

[1]G. V. Samsonov, V. I. Matkovich, P. Hagenmuller, and T. Lundstrom, *Boron and Refractory Borides* (Springer Science & Business Media, 2012).
[2]W. G. Fahrenholtz, J. Binner, and J. Zou, "Synthesis of ultra-refractory transition metal diboride compounds," J. Mater. Res. **31**, 2757 (2016).

[3]P. Vajeeston, P. Ravindran, C. Ravi, and R. Asokamani, "Electronic structure, bonding, and ground-state properties of AlB_2-type transition-metal diborides," Phys. Rev. B **63**, 045115 (2001).
[4]S. Norasetthekul, P. T. Eubank, W. L. Bradley, B. Bozkurt, and B. Stucker, "Use of zirconium diboride-copper as an electrode in plasma applications," J. Mater. Sci. **34**, 1261 (1999).
[5]W. Tan, C. A. Petorak, and R. W. Trice, "Rare-earth modified zirconium diboride high emissivity coatings for hypersonic applications," J. Eur. Ceram. Soc. **34**, 1 (2014).
[6]E. Wuchina, M. Opeka, S. Causey, K. Buesking, J. Spain, A. Cull, J. Routbort, and F. Guitierrez-Mora, "Designing for ultrahigh-temperature applications: The mechanical and thermal properties of HfB2, HfCx, HfNx and AHf(N)," J. Mater. Sci. **39**, 5939 (2004).
[7]G. S. Burkhanov and V. A. Dementiev, "Refractory monocarbides and diborides of transition metals: Promising components of high-temperature composite materials," Inorg. Mater. Appl. Res. **9**, 1012 (2018).
[8]P. H. Mayrhofer, C. Mitterer, J. G. Wen, J. E. Greene, and I. Petrov, "Self-organized nanocolumnar structure in superhard TiB_2 thin films," Appl. Phys. Lett. **86**, 131909 (2005).
[9]A. T. Lech, C. L. Turner, J. Lei, R. Mohammadi, S. H. Tolbert, and R. B. Kaner, "Superhard rhenium/tungsten diboride solid solutions," J. Am. Chem. Soc. **138**, 14398 (2016).
[10]S. Zhang, Z. Wang, P. Guo, P. Ke, M. Odén, and A. Wang, "Temperature induced superhard CrB_2 coatings with preferred (001) orientation deposited by DC magnetron sputtering technique," Surf. Coat. Technol. **322**, 134 (2017).
[11]A. I. Bazhin, A. A. Goncharov, A. D. Pogrebnyak, V. A. Stupak, and S. A. Goncharova, "Superhardness effect in transition-metal diborides films," Phys. Met. Metallogr. **117**, 594 (2016).
[12]S. Nayak, S. K. Shanmugham, I. Petrov, J. Rosen, P. Eklund, J. Birch, and A. le Febvrier, "Growth and stability of epitaxial zirconium diboride thin films on silicon (111) substrate," J. Appl. Phys. **134**, 135303 (2023).
[13]C. Schnitter, I. Petrov, I. Zhirkov, L. Hultman, J. Palisaitis, J. Rosen, and H. Högberg, "Effect of low-energy ion assistance on the properties of sputtered ZrB_2 films," Vacuum **195**, 110688 (2022).
[14]N. Hellgren, A. Sredenschek, A. Petruins, J. Palisaitis, F. F. Klimashin, M. A. Sortica, L. Hultman, POÅ Persson, and J. Rosen, "Synthesis and characterization of TiB_x ($1.2 \leq X \leq 2.8$) thin films grown by DC magnetron co-sputtering from TiB_2 and Ti targets," Surf. Coat. Technol. **433**, 128110 (2022).
[15]M. M. Dorri, J. Thörnberg, N. Hellgren, J. Palisaitis, A. Petruhins, F. F. Klimashin, L. Hultman, I. Petrov, POÅ Persson, and J. Rosen, "Synthesis and characterization of CrB_2 thin films grown by DC magnetron sputtering," Scr. Mater. **200**, 113915 (2021).
[16]M. Magnuson, L. Hultman, and H. Högberg, "Review of transition-metal diboride thin films," Vacuum **196**, 110567 (2022).
[17]S. Babar, N. Kumar, P. Zhang, J. R. Abelson, A. C. Dunbar, S. R. Daly, and G. S. Girolami, "Growth inhibitor to homogenize nucleation and obtain smooth HfB_2 thin films by chemical vapor deposition," Chem. Mater. **25**, 662 (2013).
[18]D. S. Wuu, M. L. Lee, T. Y. Lin, and R.-H. Horng, "Characterization of hafnium diboride thin film resistors by Rf magnetron sputtering," Mater. Chem. Phys. **45**, 163 (1996).
[19]W. G. Fahrenholtz and G. E. Hilmas, "Oxidation of ultra-high temperature transition metal diboride ceramics," Int. Mater. Rev. **57**, 61 (2012).
[20]T. Glechner *et al.*, "Influence of the non-metal species on the oxidation kinetics of Hf, HfN, HfC, and HfB_2 coatings," Mater. Des. **211**, 110136 (2021).
[21]J. F. Justin and A. Jankowiak, "Ultra high temperature ceramics: Densification, properties and thermal stability," AerospaceLab J. **3**, AL3 (2011).
[22]M. Mallik, A. J. Kailath, K. K. Ray, and R. Mitra, "Electrical and thermophysical properties of ZrB_2 and HfB_2 based composites," J. Eur. Ceram. Soc. **32**, 2545 (2012).
[23]S. N. Dub, S. M. Sichkar, V. A. Belous, G. N. Tolmacheva, P. I. Loboda, Y. I. Bogomol, and G. P. Kysla, "Mechanical properties of single crystals of transition metals diborides TMB_2 (TM = Sc, Hf, Zr, Ti). experiment and theory," J. Superhard Mater. **39**, 308 (2017).
[24]D. Rasic and J. Narayan, *Epitaxial growth of thin film* (Crystal Growth, 2019).
[25]Y. Yang and J. R. Abelson, "Epitaxial growth of HfB_2(0 0 0 1) on Si(0 0 1) by etching through a SiO_2 layer," J. Cryst. Growth **310**, 3197 (2008).
[26]S. Jayaraman, Y. Yang, D. Y. Kim, G. S. Girolami, and J. R. Abelson, "Hafnium diboride thin films by chemical vapor deposition from a single source precursor," J. Vac. Sci. Technol. A **23**, 1619 (2005).
[27]S. Jayaraman, J. E. Gerbi, Y. Yang, D. Y. Kim, A. Chatterjee, P. Bellon, G. S. Girolami, J. P. Chevalier, and J. R. Abelson, "Hfb_2 and Hf–B–N hard coatings by chemical vapor deposition," Surf. Coat. Technol. **200**, 6629 (2006).
[28]M. Belyansky and M. Trenary, "Heteroepitaxy of hafnium diboride on a hafnium (0001) single crystal surface," Chem. Mater. **9**, 403 (1997).
[29]J. M. Rimsza, S. C. B. Chackerian, T. J. Boyle, and B. A. Hernandez-Sanchez, "Stability evaluation of candidate precursors for chemical vapor deposition of hafnium diboride (HfB_2)," ACS Omega **6**, 11404 (2021).
[30]R. Roucka, Y.-J. An, A. V. G. Chizmeshya, V. R. D'Costa, J. Tolle, J. Menéndez, and J. Kouvetakis, "Structural and optical properties of ZrB_2 and $Hf_xZr_{1-x}B_2$ films grown by vicinal surface epitaxy on Si (1 1 1) substrates," Solid-State Electron. **52**, 1687 (2008).
[31]R. Roucka, Y. An, A. V. G. Chizmeshya, J. Tolle, J. Kouvetakis, V. R. D'Costa, J. Menéndez, and P. Crozier, "Epitaxial semimetallic $Hf_xZr_{1-x}B_2$ templates for optoelectronic integration on silicon," Appl. Phys. Lett. **89**, 242110 (2006).
[32]J. V. Dilorenzo, "Vapor growth of epitaxial GaAs: A summary of parameters which influence the purity and morphology of epitaxial layers," J. Cryst. Growth **17**, 189 (1972).
[33]S. Wang, A. Roy, and K. Komvopoulos, "Thermal stability and diffusion characteristics of ultrathin amorphous carbon films grown on crystalline and nitrogenated silicon substrates by filtered cathodic vacuum arc deposition," Sci. Rep. **11**, 13106 (2021).
[34]A. K. Sinha, H. J. Levinstein, and T. E. Smith, "Thermal stresses and cracking resistance of dielectric films (SiN, $Si3N_4$, and SiO_2) on Si substrates," J. Appl. Phys. **49**, 2423 (1978).
[35]A. A. Goncharov, S. N. Dub, and A. V. Agulov, "Structure, composition, and physicomechanical characteristics of HfB_2 and Hf-B-N films," Phys. Met. Metallogr. **114**, 95 (2013).
[36]J. M. Eldridge, A. R. Forouhi, G. L. Gorman, and J. O. Moore, "Various properties of sputter-deposited HfB_2 films," J. Electrochem. Soc. **137**, 3905 (1990).
[37]A. Le Febvrier, L. Landälv, T. Liersch, D. Sandmark, P. Sandström, and P. Eklund, "An upgraded ultra-high vacuum magnetron-sputtering system for high-versatility and software-controlled deposition," Vacuum **187**, 110137 (2021).
[38]M. Mayer, "SIMNRA, a simulation program for the analysis of NRA, RBS and ERDA," AIP Conf. Proc. **475**, 541–544 (1999).
[39]P. Ström, P. Petersson, M. Rubel, and G. Possnert, "A combined segmented anode gas ionization chamber and time-of-flight detector for heavy Ion elastic recoil detection analysis," Rev. Sci. Instrum. **87**, 103303 (2016).
[40]M. V. Moro, R. Holeňák, L. Z. Medina, U. Jansson, and D. Primetzhofer, "Accurate high-resolution depth profiling of magnetron sputtered transition metal alloy films containing light species: A multi-method approach," Thin Solid Films **686**, 137416 (2019).
[41]K. Arstila *et al.*, "Potku—New analysis software for heavy ion elastic recoil detection analysis," Nucl. Instrum. Methods Phys. Res., B **331**, 34 (2014).
[42]K. Arstila, T. Sajavaara, and J. Keinonen, "Monte Carlo simulation of multiple and plural scattering in elastic recoil detection," Nucl. Instrum. Methods Phys. Res., B **174**, 163 (2001).
[43]I. Horcas, R. Fernández, J. M. Gómez-Rodríguez, J. Colchero, J. Gómez-Herrero, and A. M. Baro, "WSXM: A software for scanning probe microscopy and a tool for nanotechnology," Rev. Sci. Instrum. **78**, 13705 (2007).
[44]ICDD—The International Centre for Diffraction Data. Silicon (Si) PDF Number:00-027-1402 (n.d.).
[45]ICDD—The International Centre for Diffraction Data. Hafnium Diboride (HfB_2) PDF Number: 00-038-1398 1986 (n.d.).
[46]ICDD—The International Centre for Diffraction Data. Hafnium Oxide (HfO2) PDF Number: 00-038-0104 2010 (n.d.).

[47]ICDD—The International Centre for Diffraction Data. Hafnium Boride (HfB) PDF Number: 01-077-7066 1967 (n.d.).
[48]ICDD—The International Centre for Diffraction Data. Hafnium Carbide (HfC) PDF Number: 00-039-1491 (n.d.).
[49]P. Rogl and H. Bittermann, "On the ternary system hafnium–boron–carbon," J. Solid State Chem. **154**, 257 (2000).
[50]See https://Next-Gen.Materialsproject.Org/Phasediagram for phase diagram obtained from the web application of https://next-gen.materialsproject.org/ revealed that HfBC (sg: $P6_3/mmc$) is 0.547 eV/atom above the convex hull with a formation enthalpy of −0.275 eV/atom. The closest thermodynamically stable compositions are HfB_2 (sg: P6/mmm), B_4C (sg: C1m1), and HfC (sg: $Fm\bar{3}m$). The formation enthalpies of HfB_2, B_4C, and HfC are computed as −1.018 eV/atom, −0.1 eV/atom, and -0.939 eV/atom, respectively.
[51]A. Jain, G. Hautier, S. Ong, C. Moore, C. Fischer, K. Persson, and G. Ceder, "Formation enthalpies by mixing GGA and GGA+U calculations," Phys. Rev. B **84**, 45115 (2011).
[52]G. Abrasonis, G. J. Kovács, L. Ryves, M. Krause, A. Mücklich, F. Munnik, T. W. H. Oates, M. M. M. Bilek, and W. Möller, "Phase separation in carbon-nickel films during hyperthermal ion deposition," J. Appl. Phys. **105**, 083518 (2009).
[53]Z. J. Liu and Y. G. Shen, "Temperature effect on surface roughening of thin films," Surf. Sci. **595**, 20 (2005).
[54]Z. Ghorannevis, M. T. Hosseinnejad, M. Habibi, and P. Golmahdi, "Effect of substrate temperature on structural, morphological and optical properties of deposited Al/ZnO films," J. Theor. Appl. Phys. **9**, 33 (2015).
[55]J. Kouvetakis, Y. J. An, V. R. D'Costa, J. Tolle, A. V. G. Chizmeshya, J. Menéndez, and R. Roucka, "Synthesis of (Hf, Zr)B_2-based heterostructures: Hybrid substrate systems for low temperature Al–Ga–N integration with Si," J. Mater. Chem. **18**, 4775 (2008).
[56]J. Tolle, R. Roucka, I. S. T. Tsong, C. Ritter, P. A. Crozier, A. V. G. Chizmeshya, and J. Kouvetakis, "Epitaxial growth of group III nitrides on silicon substrates via a reflective lattice-matched zirconium diboride buffer layer," Appl. Phys. Lett. **82**, 2398 (2003).
[57]R. Trivedi, P.-L. Liu, R. Roucka, J. Tolle, A. V. G. Chizmeshya, I. S. T. Tsong, and J. Kouvetakis, "Mismatched heteroepitaxy of tetrahedral semiconductors with Si via ZrB_2 templates," Chem. Mater. **17**, 4647 (2005).